Journal of Power Sources 209 (2012) 147–151

Contents lists available at SciVerse ScienceDirect

Journal of Power Sources

journal homepage: www.elsevier.com/locate/jpowsour

Short communication

Proton transport resistance correlated to liquid water content of gas diffusion layers

Jon P. Owejan*, Jeffrey J. Gagliardo, Robert C. Reid, Thomas A. Trabold[1]

General Motors Electrochemical Energy Research Lab, 10 Carriage Street, Honeoye Falls, NY 14472, United States

ARTICLE INFO

Article history:
Received 26 December 2011
Received in revised form 19 February 2012
Accepted 20 February 2012
Available online 1 March 2012

Keywords:
Fuel cells
Water transport
Neutron imaging
Current distribution
Proton resistance
Flooding

ABSTRACT

Proton transport resistance in the polymer electrolyte of proton exchange membrane fuel cells (PEMFCs) is a significant contributor to ohmic overpotential. Conductivity is largely controlled by water uptake, which requires a delicate water balance to avoid an increase in mass transport overpotential due to diffusion resistance in porous components. The present work explores this relationship with distributed liquid water and high frequency resistance (HFR) measurements. The HFR response to local changes in liquid water content is characterized for two gas diffusion layers (GDLs) with different thermal resistivities. From these experiments, it is shown that liquid water must be present in the gas diffusion layer (GDL) to minimize the HFR. Furthermore, the impact of varied saturation levels induced by GDL thermal gradients on drying transients is considered with both in-plane and through-plane neutron imaging.

1. Introduction

PEMFC water management is a broad research topic because of the wide range of length scales present in a fuel cell stack. Researchers must consider transport from the molecular scale in the polymer electrolyte, to droplet formation in the diffusion layer pore structure, to small slugs of water in the bipolar plate channels, to larger slugs (on the scale of centimeters) accumulating in the bipolar plate manifolds and ancillary equipment. If water was not required to facilitate proton conduction between the anode and cathode catalyst sites, operating conditions could easily be prescribed to enable removal of all product water in the vapor phase. However, the current state-of-the-art in membrane materials clearly indicates that first-generation PEMFC systems with acceptably high performance at reasonable cost will require a humid operating environment that results in water condensation at low stoichiometric ratios.

The relationship between liquid water accumulation and transport resistance has been widely studied with both direct and indirect diagnostic methods. In a recent review of electrochemical and physical diagnostic methods, Wu et al. presented many of these techniques and the conclusions based on them [1,2]. From a commercial stack perspective, the majority of water transport research is related to the water activity required for membrane hydration. The relationship between the proton transport resistance and operating parameters has been widely studied with impedance in the high frequency spectrum [3–5]. Liquid water, which can block gas transport (observed via direct visualization techniques), can be problematic during operation at high relative humidity (RH) – a condition which is required to minimize proton resistance [6]. The trade-off between too much water (high oxygen transport resistance) and too little water (high proton transport resistance) results in optimum performance near a water balance independent combined anode and cathode exhaust stream RH of 100%, as maximum membrane conductivity is achieved while avoiding severe mass transport loss associated with excessive liquid water [7].

Combining visualization with local current and impedance measurements has enabled researchers to investigate the relationship between liquid water accumulation and local performance loss [8–10]. These experiments universally demonstrate that severe water accumulation negatively impacts local current output. Many researchers generalize any liquid water content in the carbon fiber substrate as 'flooding', which has a negative connotation. However, these studies did not consider the optimum saturation (the fraction of pore volume in the compressed substrate that contains liquid water), as the presence of some liquid water might be necessary to reduce proton transport resistance to a minimum value for a given membrane and ionomer type. If this is the case, the gas diffusion layer (GDL) should be designed to maintain a low, but non-zero, level of saturation.

* Corresponding author. Tel.: +1 585 953 5558; fax: +1 585 624 6686.
E-mail address: jon.owejan@gm.com (J.P. Owejan).
[1] Current address: Golisano Institute for Sustainability, Rochester Institute of Technology, 111 Lomb Memorial Drive, Rochester, NY 14623, United States.

0378-7753/$ – see front matter © 2012 Elsevier B.V. All rights reserved.
doi:10.1016/j.jpowsour.2012.02.087

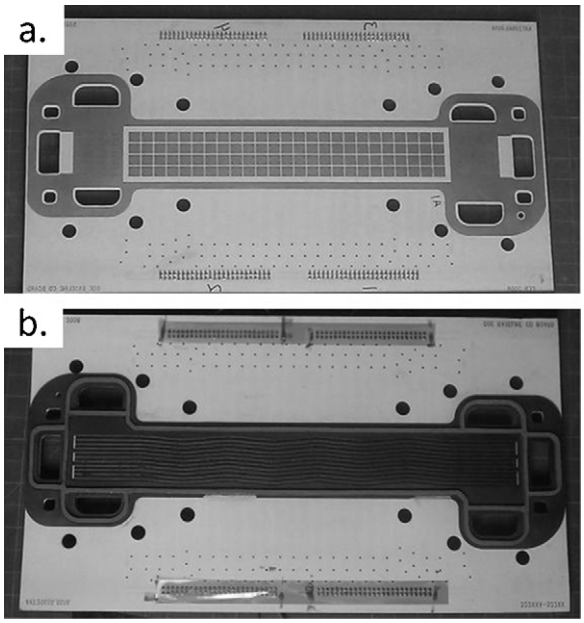

Fig. 1. Distributed measurement tool, (a) printed circuit board, (b) composite flow field plate bonded to board.

In the current work we use the thermal resistivity of the GDL to impact water saturation level and correlate these changes to the proton transport resistance in the membrane. Expanding on previous work [8,9], we have developed an unique combination of experiments and analyses to consider the proton transport resistance associated with liquid water accumulation, as it is known that proton resistance in perfluorosulfonic acid solid electrolyte is only minimized if some liquid water is present [11,12]. By monitoring distributed high-frequency resistance (HFR) and local liquid water content during transient drying, this article considers the saturation level required to maximize ionic conductivity in the membrane, and how it relates to the magnitude of saturation in the GDLs.

2. Experimental

The experimental work conducted in this study combined a small-scale fuel cell with distributed HFR measurements and neutron imaging. A fuel cell test stand with individually calibrated control parameters was used to operate test cells. The PEMFC test fixture was specifically designed within commercial stack constraints to provide pure counter-flow in the active area where anode and cathode gas flow is parallel in opposite directions. This design is described in detail by Owejan et al. [9].

2.1. Current distribution measurement

The fuel cell current distribution tool consisted of a printed circuit board with isolated contacts that redirect current through shunt resistors. The circuits were printed on a polytetrafluoroethylene (PTFE) substrate to improve neutron transmission in a similar manner to work reported by Gagliardo et al. [8]. As shown in Fig. 1a, the measurement array consisted of 25 columns down-the-channel with 4 rows across the channels and lands. The voltage response across each shunt was measured with a separate data acquisition channel. The flow field was machined in thin graphite composite resin and bonded to the distributed measurement board (Fig. 1b). The continuous flow field results in slight "blurring" of current between segments but this will be no larger than the 1.5 mm thickness of the plate. The plate was verified to be isopotential by monitoring voltage along the perimeter at varying distances from an applied current.

To measure the high frequency impedance component associated with the zero-phase resistance, the current was perturbated at a frequency of 1 kHz with a peak-to-peak amplitude of 500 mA. At this high frequency, the voltage and current were assumed to be in phase and ohmic resistance was calculated based on the voltage response, assumed constant for all segments (isopotential plate) relative to the individual current response which varied based on the resistance of each segment.

Table 1
Measured diffusion and thermal parameters for the GDL material studied [13–15].

Parameter	TGP-H-060	Grafil U-105	Unit
Thermal resistivity [13]	3.1 ± 0.3	9.2 ± 0.3	$cm^2\,K\,W^{-1}$
Effective diffusion coefficient [14]	0.036 ± 0.002	0.037 ± 0.002	$cm^2\,s^{-1}$
Uncompressed thickness	225 ± 12	230 ± 10	μm
Electrical Resistivity [15]	7.8	13.3	mΩ cm
Porosity	66%	73%	–

2.2. Materials

Two GDL substrates with different thermal conductivities but similar diffusion resistances were selected to demonstrate how through-plane thermal gradients impact liquid water content in the GDL. By varying the GDL thermal conductivity the fuel cell water content could be altered at a given operating condition, thus establishing the correlation between liquid water quantity and membrane resistance. The high and low thermal conductivity GDLs selected for this study were Toray TGP-H-060 and Mitsubishi Rayon Corp. (MRC) Grafil U-105, respectively. Each sample was prepared with 7 wt% PTFE in the substrate and a 30 μm thick microporous layer consisting of an 8:1:1 carbon:PTFE:FEP ratio. The relevant measured parameters for the resulting GDLs are listed in Table 1. The GDLs were compressed to 20% strain based on the measured uncompressed thickness. All experiments were run with an 18 μm thick membrane and 0.2/0.3 mg Pt cm^{-2} anode/cathode catalyst loading membrane electrode assembly (MEA) manufactured by W.L. Gore.

3. Results and discussion

The GDLs being compared in this study were expected to exhibit different water accumulation behavior at higher temperature operating conditions due to the temperature gradient that exists between the coolant fluid and the cathode catalyst layer [16]. As water condenses in the porous medium, the temperature gradient will dictate the location of the condensing liquid front. Hence, a lower temperature gradient will result in more liquid water volume, all else held constant (diffusion properties, for example). This behavior was confirmed with in situ neutron imaging at the National Institute of Standards and Technology (NIST) Neutron Imaging Facility (NIF) by measuring the integrated liquid water thickness through all layers with the neutron beam perpendicular to the active area plane [9]. Shown in Figs. 2 and 3 is a comparison of liquid water content and performance for the Toray and MRC GDLs at various current densities during a polarization curve acquired at 80 °C cell temperature. The similar polarization performance with a nearly factor of two difference in liquid water volume indicates that GDL water content can have an insignificant influence on fuel cell performance for certain operating conditions.

The data shown in Fig. 4 at 80 °C demonstrate the contrast in liquid water accumulation due to the nonlinear relationship between saturation vapor pressure and temperature. As stated above, even though there is a factor of approximately two difference in water

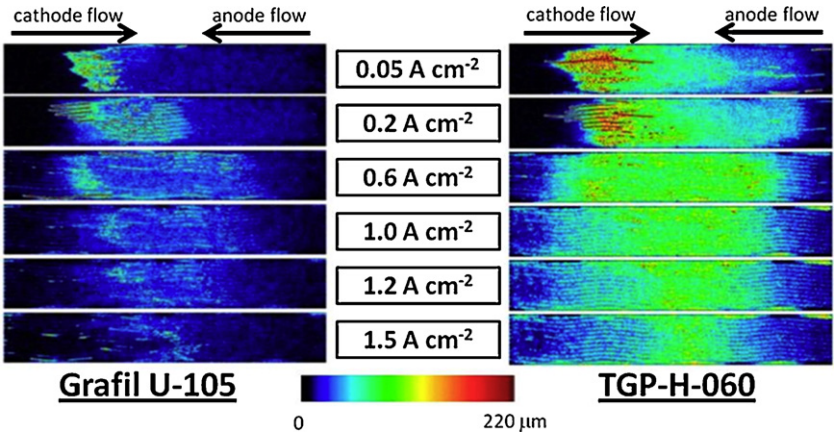

Fig. 2. Comparison of liquid water accumulation in MRC and Toray GDL (80 °C, 1.5/2.0 H_2/air stoichiometry, 95% inlet RH, 200 kPa abs. outlet pressure, counter-flow).

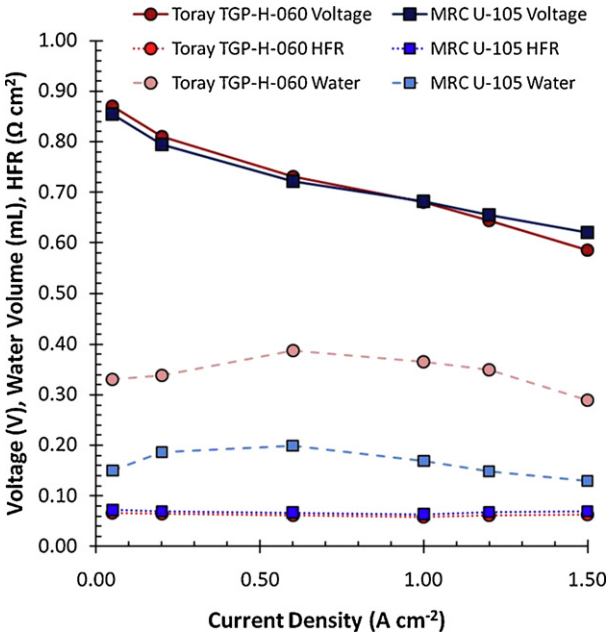

Fig. 3. Performance comparison of Toray and MRC GDLs (80 °C, 1.5/2.0 H_2/air stoichiometry, 95% inlet RH, 150 kPa abs. outlet pressure, counter-flow).

content at all current densities for 80 °C cell temperature, the voltage and HFR measurements are nearly identical (Fig. 3). Only at the 1.5 A cm^{-2} condition is there some evidence of greater mass transport loss in the cell with high thermal conductivity GDL material. To further demonstrate that water accumulation in the bulk of the GDL is mainly related to the induced temperature gradient between the cathode catalyst layer and coolant, the liquid water content at 35 and 80 °C is presented in Fig. 4. For each of these measured water distributions, the associated temperature gradients were calculated based on the thermal resistivities in Table 1 and the heat flux at 1.5 A cm^{-2} determined from the overpotentials in Fig. 3. At 35 °C a difference of 1.5 kPa in saturation vapor pressure gradient results from temperature gradients of 2 and 6 °C for Toray and MRC papers respectively. Conversely, at 80 °C the difference in induced temperature gradient for the two materials results in a difference of 8.8 kPa in saturation vapor pressure gradient. Consequently, the total water content for the Toray material is less dependent on cell temperature. However, the in-plane liquid water content along the channel direction is clearly influenced in Fig. 4. At 80 °C, the liquid water is more concentrated at the center of the active area while the anode and cathode inlet regions remain relatively dry. This temperature dependence is later used to consider variations in GDL water content at the same operating condition.

This relationship between accumulated water and performance was explored further by monitoring local HFR relative to liquid water content for the cell assembled with MRC GDL (Fig. 5). Here, the neutron image was analyzed over discrete areas aligned with the segmentation of the current distribution tool shown in Fig. 1. Each water thickness measurement is the integrated liquid water measured per pixel that is averaged over an area equivalent to the current measurement segment. The plot shown in Fig. 5 demonstrates the strong dependence between bulk water in the GDL and membrane proton resistance that is governed by its hydration level. For this plot, the gradient in water thickness values was achieved by preconditioning the cell at a wet condition (35 °C, 0.4 A cm^{-2}, 150 kPa outlet pressure, 2/2 H_2/air stoichiometric ratios) then purging at a drier exit condition (35 °C, 0.1 A cm^{-2}, 101 kPa outlet pressure, 2/16 H_2/air stoichiometric ratios). At this low temperature condition, the cathode purge dries the cell slowly (~10 min), thus allowing several levels of liquid water thickness to be captured with 30 s neutron integration times in each segment. The inset

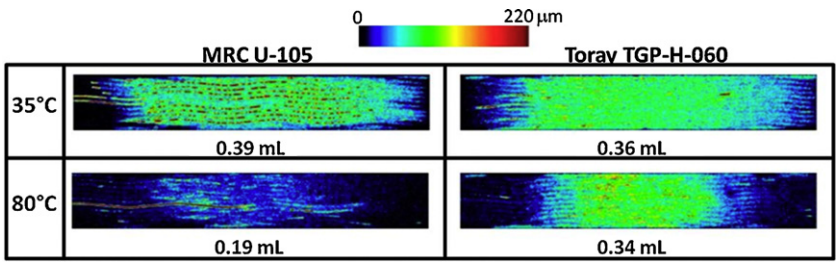

Fig. 4. Impact of GDL induced thermal gradient on measured water volume at 35 and 80 °C (0.4 A cm^{-2}, 1.5/2.0 H_2/air stoichiometry, 95% inlet RH, 150 kPa abs. outlet pressure, counter-flow).

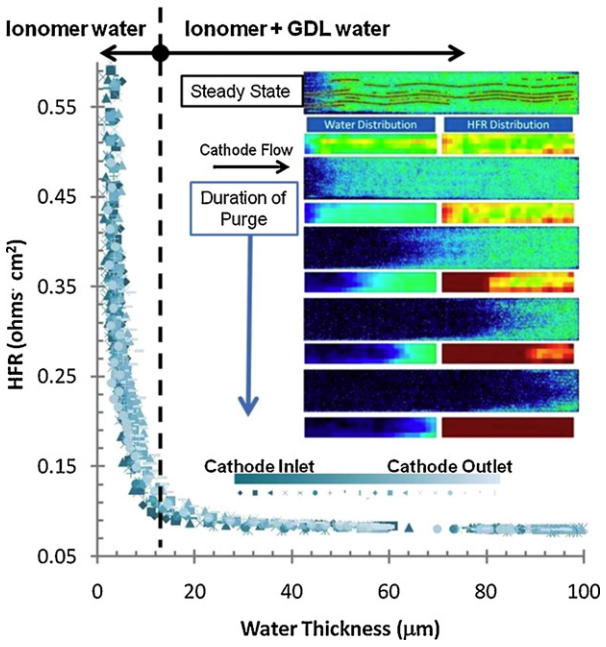

Fig. 5. HFR response to local water thickness during a slow drying transient; liquid equilibrated equivalent liquid water thickness in the ionomer is indicated by the vertical dashed line. Neutron images, binned water thickness and HFR distributions that represent data are also shown. Precondition: 35 °C, 0.4 A cm^{-2}, 150 kPa abs. outlet pressure, 2/2 H_2/air stoichiometric ratios; drying condition: 35 °C, 0.1 A cm^{-2}, 101 kPa abs. outlet pressure, 2/16 H_2/air stoichiometric ratios.

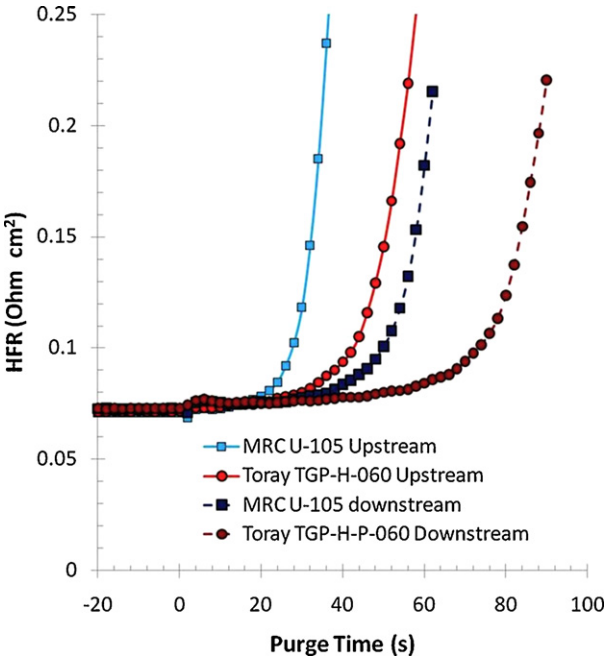

Fig. 6. Drying transient comparing HFR response for Toray and MRC GDLs. Precondition: 80 °C, 0.4 A cm^{-2}, 150 kPa abs. outlet pressure, 2/2 H_2/air stoichiometric ratios; drying condition: 80 °C, 0.1 A cm^{-2}, 101 kPa abs. outlet pressure, 2/16 H_2/air stoichiometric ratios.

neutron images and distributed HFR in Fig. 5 demonstrate this drying, as a front, moving from the cathode inlet to outlet during the length of the purge. These experiments were run under a wide array of conditions, and the same general trend in HFR was observed as integrated liquid water thickness decreased.

In Fig. 5, the sharp increase in HFR as water thickness approaches a value that is associated with liquid equilibrated ionomer water content (an estimated 13 μm equivalent water thickness for the 950 equivalent weight membrane at 20 moles water per acid site) is somewhat obvious given the strong dependence of the ionomer "lambda" value (number of water molecules per sulfonate site) on the phase of water. However, what is unique about these data is that the HFR asymptote indicates only a small amount of liquid water in the GDL is required to maintain the ionomer lambda value at a liquid equilibrated state.

This difference in water storage capacity realized by GDL thermal properties can have varying impacts on fuel cell system performance. On one hand, a higher stored volume of liquid water can buffer high load and temperature transients. On the other hand, a lower stored volume can shorten the freeze preparation purge, thereby reducing hydrogen consumption. We explore this further by comparing the local HFR response of the two GDLs selected for this study during a drying transient at 80 °C. Data are presented for segments of the HFR distribution board at both upstream and downstream locations, 1.4 and 16.9 cm, respectively, from the cathode inlet edge of the active area. The HFR response in Fig. 6 clearly demonstrates this trade-off where the upstream and downstream HFR transients are much slower for Toray relative to MRC GDLs. With regard to purge energy this delays the rapid increase in HFR (indicative of substantial drying in the MEA) for the less thermally resistive Toray GDL by as much as 25 s at the downstream location, which translates to a significant efficiency loss as compared to the MRC GDL. In practice, the longer shutdown purge duration required for the Toray material could be balanced by the benefit of increased robustness to long excursions at dry operating conditions. The sensitive relationship shown in Fig. 6 is important when selecting GDL materials for a specific application or to optimize a specific region of the operating space.

Finally, the integrated water measurement presented thus far is ignoring the anode vs. cathode distribution in these two experimental configurations. To elucidate this we applied high resolution neutron imaging methods to measure the through-plane water content by orienting the cell such that the neutron path was parallel to the active area plane [17]. This comparison is provided in Fig. 7,

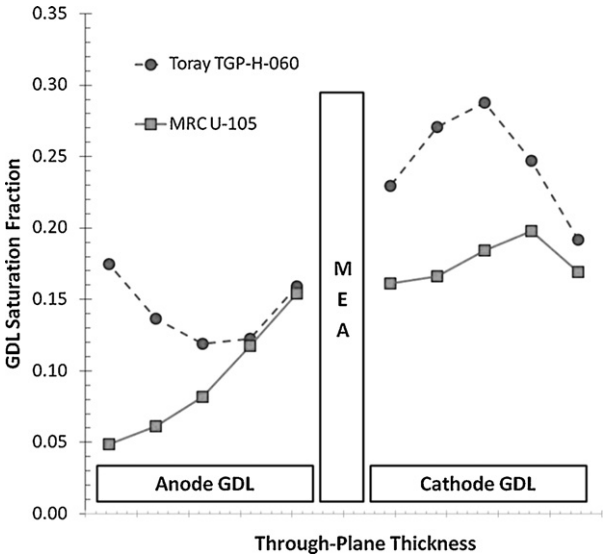

Fig. 7. High resolution neutron imaging of through-plane water profiles for Toray (80 °C, 0.6 A cm^{-2}, 4/4 H_2/air stoichiometry, 95% inlet RH, 150 kPa abs. outlet pressure, counter-flow).

where integrated liquid water thickness is scaled to GDL saturation. Here it is observed that the increased overall water content with the Toray material is a result of both a change in the anode distribution, where more water is stored toward the anode flow field and an increase in cathode GDL liquid water content with a similar distribution. This result indicates a shift in the overall water balance, which correlates to the slower HFR response of Toray observed in Fig. 6, as the additional anode water removal by the cathode gas stream is slowed by the membrane. Also, an increase in anode water further complicates the trade-offs mentioned previously, because draining water from the anode subsystem can impact system efficiency.

4. Conclusions

The relationship between GDL saturation and proton transport resistance was examined with local measurements of liquid water and HFR by considering GDLs with different thermal conductivities. Experiments comparing Toray with MRC GDLs yield similar polarization performance to 1.5 A cm^{-2} while the 3× higher thermal resistance MRC material retains significantly less liquid water at 80 °C. This difference in water content at the same operating condition was used to consider how local GDL saturation impacts proton transport resistance in the membrane. Results show that this relationship is very sensitive, and a small amount of liquid water in the GDL is required to minimize proton transport resistance, but as saturation increases beyond this value, the proton transport resistance remains constant. Through-plane liquid water distribution and transient drying experiments highlight the practical trade-off associated with this relationship. A lower thermal resistance GDL can result in higher anode and cathode GDL liquid water content, providing a water buffer for dry transients but also increases required purge energy for reliable cold starts in automotive applications.

Acknowledgments

This work was supported in part by the U.S. Department of Energy under contracts DE-FG36-07G017018 and DE-EE0000470. David Jacobson, Daniel Hussey and Eli Baltic are acknowledged for their work developing neutron imaging facilities and methods for fuel cell research that were applied here.

References

[1] J. Wu, X.-Z. Yuan, H. Wang, M. Blanco, J.J. Martin, J. Zhang, Int. J. Hydrogen Energy 33 (2008) 1735–1746.
[2] J. Wu, X.-Z. Yuan, H. Wang, M. Blanco, J.J. Martin, J. Zhang, Int. J. Hydrogen Energy 33 (2008) 1747–1757.
[3] R. Makharia, M.F. Mathias, D.R. Baker, J. Electrochem. Soc. 152 (2005) A970–A977.
[4] J.M. Le Canut, R.M. Abouatallah, D.A. Harrington, J. Electrochem. Soc. 153 (2006) A857–A864.
[5] S.K. Roy, H. Hagelin-Weaver, M.E. Orazem, J. Power Sources 196 (2011) 3736–3741.
[6] A. Bazylak, Int. J. Hydrogen Energy 34 (2009) 3845–3857.
[7] W. Schmittinger, A. Vahidi, J. Power Sources 180 (2008) 1–14.
[8] J.J. Gagliardo, J.P. Owejan, T.A. Trabold, T.W. Tighe, Nucl. Instrum. Method Phys. Res. A 605 (2009) 115–118.
[9] J.P. Owejan, J.J. Gagliardo, J.M. Sergi, T.A. Trabold, S.G. Kandlikar, Int. J. Hydrogen Energy 34 (2009) 3436–3444.
[10] F.B. Weng, C.Y. Hsu, C.W. Lei, Int. J. Hydrogen Energy 35 (2010) 3664–3675.
[11] T.A. Zawodzinski Jr., C. Derouin, S. Radzinski, R.J. Sherman, V.T. Smith, T.E. Springer, S. Gottesfeld, J. Electrochem. Soc. 140 (1993) 1041–1047.
[12] W. Dai, H. Wang, X-Z. Yuan, J.J. Martin, D. Yang, J. Qiao, J. Ma, Int. J. Hydrogen Energy 34 (2009) 9461–9478.
[13] D.W. Fultz, P.A. Chuang, ASME J. Fuel Cell Sci. Technol. 8 (2011), 041010-1–6.
[14] D.R. Baker, D.A. Caulk, K.C. Neyerlin, M.W. Murphy, J. Electrochem. Soc. 156 (2009) B991–B1003.
[15] M. Mathias, J. Roth, J. Fleming, W. Lehnert, in: W. Vielstich, A. Lamm, H.A. Gasteiger (Eds.), Handbook of Fuel Cells: Fundamentals, Technology, Applications, John Wiley and Sons, New York, 2003.
[16] J.P. Owejan, J.E. Owejan, W. Gu, T.A. Trabold, T.W. Tighe, M.F. Mathias, J. Electrochem. Soc. 157 (2010) B1456–B1464.
[17] D.S. Hussey, D.L. Jacobson, M. Arif, J.P. Owejan, J.J. Gagliardo, T.A. Trabold, J. Power Sources 172 (2007) 225–228.